

**This work has been submitted to the IEEE for possible publication.
Copyright may be transferred without notice, after which this
version may no longer be accessible.**

A Graphical Method for Designing Time-Optimal Non-Cartesian Gradient Waveforms

Rui Luo, Hongzhang Huang, Qinfang Miao, Jian Xu, Peng Hu, Haikun Qi

Abstract—One of the fundamental challenges for non-Cartesian MRI is the need of designing time-optimal and hardware-compatible gradient waveforms for the provided k -space trajectory. Currently dominant methods either work only for certain trajectories or require significant computation time. In this paper, we aim to develop a fast general method that is able to generate time-optimal gradient waveforms for arbitrary non-Cartesian trajectories satisfying both slew rate and gradient constraints. In the proposed method, the gradient waveform is projected into a space defined by the gradients along the spatial directions, termed as g -space. In the constructed g -space, the problem of finding the next gradient vector given the current gradient vector under desired slew rate limit and with desired direction is simplified to finding the intersection between a line and a circle. To handle trajectories with increasing curvature, a Forward and Backward Sweep (FBS) strategy is introduced, which ensures the existence of the solution to the above mentioned geometry problem for arbitrary trajectories. Furthermore, trajectory reparameterization is proposed to ensure trajectory fidelity. We compare the proposed method with the previous optimal-control method in simulations and validate its feasibility for real MR acquisitions in phantom and human knee for a wide range of non-Cartesian trajectories. The proposed method enables accurate and fast gradient waveform design, achieving significant reduction in computation time and slew rate overshoot compared to the previous method. The source code will be publicly accessible upon publication of this study.

Index Terms—Non-Cartesian Imaging, Gradient Waveform, k -space Trajectory, Magnetic Resonance Imaging, g -space

I. INTRODUCTION

NON-Cartesian imaging has been widely applied in Magnetic Resonance Imaging (MRI) applications such as quantitative mapping, dynamic imaging, silent imaging, and Magnetic Resonance Spectroscopy Imaging, due to its efficient sampling patterns, motion robustness, high signal-to-noise ratio (SNR), and incoherent undersampling artifacts [1]–[7]. A fundamental challenge in non-Cartesian imaging is the need of designing a readout gradient waveform for the desired trajectory that not only satisfies the hardware constraints but also ensures the time optimality.

A. Prior Work

In the early years, when only a few non-Cartesian trajectories were available, methods of designing optimal gradient waveforms were often focused on certain specific trajectory such as the commonly adopted spiral [8], [9] or rosette [10] trajectories. The basic idea is to model the slew rate with the trajectory parameter, and then solve for the trajectory parameter under the desired slew rate amplitude. Meyer et al. proposed a fast method for designing the spiral trajectory [11], which starts with some initial gradient and calculates the gradient vector for the next time point by first determining its direction (the first derivative of the trajectory) and then calculating the maximum allowable magnitude as the intersection of a line parallel to the determined gradient direction and a circle representing the slew rate constraint. Calculating the gradients successively for increasing time points yields the time-optimal gradient waveforms. By taking advantage of the geometry of the problem, this method provides an analytical and non-iterative solution to the gradient waveform design for various spiral trajectories. However, for more complex trajectories such as those with increasing curvature or end up with zero gradient amplitude, this method of evaluating the gradients by running time forward only cannot predict upcoming curvature maxima, resulting in an unsolvable problem. Moreover, in the geometric solution, constraining only the direction of the next gradient vector to be parallel to the current trajectory tangent may lead to trajectory drift and compromise the generated trajectory accuracy.

Subsequently, Lustig et al. introduced a method based on the optimal control theory that constrains both the gradient

Manuscript submitted July 10, 2025. This work was supported in part by the High Technology Research and Development Center of the Ministry of Science and Technology of China under Grant SQ2022YFC2400133, in part by the Explorer Program of Shanghai Municipality under Grant 23TS1400300. (Corresponding author: Haikun Qi.)

Rui Luo is with the School of Biomedical Engineering & State Key Laboratory of Advanced Medical Materials and Devices, ShanghaiTech University, Shanghai 201210, China (e-mail: luorui2023@shanghaitech.edu.cn).

Hongzhang Huang is with the School of Biomedical Engineering & State Key Laboratory of Advanced Medical Materials and Devices, ShanghaiTech University, Shanghai 201210, China (e-mail: huangzh2023@shanghaitech.edu.cn).

Qinfang Miao is with the School of Biomedical Engineering & State Key Laboratory of Advanced Medical Materials and Devices, ShanghaiTech University, Shanghai 201210, China (e-mail: miaoqf2022@shanghaitech.edu.cn).

Jian Xu is with UIH America, Inc., Houston, TX 77054, USA (e-mail: jian.xu01@united-imaging.com).

Peng Hu is with the School of Biomedical Engineering & State Key Laboratory of Advanced Medical Materials and Devices, ShanghaiTech University, Shanghai 201210, China (e-mail: hupeng@shanghaitech.edu.cn).

Haikun Qi is with the School of Biomedical Engineering & State Key Laboratory of Advanced Medical Materials and Devices, ShanghaiTech University, Shanghai 201210, China (e-mail: qihk@shanghaitech.edu.cn).

and slew rate amplitudes [12]. This method is non-iterative and applicable to arbitrary non-Cartesian trajectories. A key improvement of Lustig's approach compared to Meyer's is the adoption of a Forward and Backward Sweep (FBS) strategy, which solves for the gradient amplitude both forward and backward in the first step, and takes the minimum of the two solutions in the second to ensure proper deceleration before reaching the curvature maxima. The FBS strategy enables handling of arbitrary trajectories, where curvature is not monotonic, and has been widely adopted for designing gradient waveforms for various non-Cartesian trajectories [7], [13]–[15].

Although widely employed, there are some limitations in Lustig's method. The optimal control algorithm accepts only arc-length parameterized trajectories, requiring additional arc-length integration and numerical inversion to convert arbitrary parameterization to arc-length parameterization, which introduces significant computational overhead and prevents the application of this method to real-time gradient calculation for trajectories with randomly varied shapes. Another limitation is the inaccurate slew rate control. Since the derived gradients from the optimal control algorithm are parameterized by arc-length rather than by time, converting the algorithm output to scanner-executable gradient waveforms requires additional interpolation. Inconsistent densities between arc-length samples and time samples result in inconsistent interpolation accuracy, which in turn causes the slew rate in low-gradient regions, such as at the beginning of a gradient waveform, to exceed the inputted slew rate limit. This issue may cause the scan failure, especially when the target slew rate is close to the hardware limit. This can be a severe problem in the clinical setting. There are also other works that have attempted to address the non-Cartesian gradient design problem. However, those methods either need to modify the target trajectory [16], [17] or require computationally expensive iterative optimization [18], [19] that is more time-consuming than Meyer's and Lustig's non-iterative methods.

B. Contribution

In this paper, we propose to transform the gradient waveforms to a space defined by the gradients along the x-, y- and z-directions, termed as g -space. Similar to Meyer's method, the gradients can be solved for analytically and graphically in the constructed g -space. To be applicable to arbitrary trajectories, we propose to integrate the FBS strategy into the graphical method. Furthermore, a reparameterization method is proposed to ensure trajectory accuracy. The main advantages of the proposed approach are the following: i) The designed gradient waveforms are time-optimal under both gradient and slew rate limits. ii) The proposed method applies to any trajectory. iii) The derived k -space sampling points are exactly on the trajectory defined by the inputted trajectory function. iv) The proposed method is simple and thus much faster than the previous optimal control method. v) Each gradient vector is paired with a trajectory parameter, which is useful for trajectory segmentation.

C. Paper Organization

In Section II, we review the formulation of MRI acquisition, and provide the definitions of trajectory, gradient and slew rate. Subsequently, we introduce the transformation from gradient waveforms to g -space, and explain the advantage of using g -space representation. We further elucidate the solutions in the previous graphical method, and point out in which situation there will be no solution. Then we solve this problem by introducing the FBS strategy. At the end of this section we point out another key limitation of the previous graphical method and address it by making use of the trajectory parameter sequence which is calculated simultaneously with the gradient series. In Section III, we describe the conducted experiments to validate the performance of the proposed method for various non-Cartesian trajectories, and the feasibility of using this method for real non-Cartesian MRI. In Section IV, we report the simulation and real MRI scan results. In Section V, we discuss the potential and influence of the proposed method.

II. THEORY

In this section, we elaborate on the full mathematical derivation of the proposed method. Without loss of generality, the figures and derivations are presented for the 2D trajectory, while all formulations and solutions also apply to 3D trajectories.

A. From Trajectory to Slew Rate

In MRI, the k -space sampling position $\mathbf{k}(t)$ is given by

$$\mathbf{k}(t) = \gamma \int_0^t \mathbf{g}(\tau) d\tau, \quad (1)$$

where $\mathbf{g}(t)$ is the gradient and γ is the gyromagnetic ratio. For notational simplicity, we absorb the gyromagnetic ratio γ into the gradient, yields:

$$\mathbf{k}(t) = \int_0^t \mathbf{g}(\tau) d\tau, \quad (2)$$

The slew rate $\mathbf{s}(t)$ is defined as

$$\mathbf{s}(t) = \frac{d\mathbf{g}(t)}{dt}. \quad (3)$$

It follows that $\mathbf{k}(t)$, $\mathbf{g}(t)$, and $\mathbf{s}(t)$ are related as successive derivatives:

$$\mathbf{g}(t) = \frac{d\mathbf{k}(t)}{dt}, \quad (4)$$

$$\mathbf{s}(t) = \frac{d^2\mathbf{k}(t)}{dt^2}. \quad (5)$$

For a given gradient coil, hardware constraints apply:

$$\forall t: \quad |\mathbf{g}(t)| < G_{\text{lim}}, \quad |\mathbf{s}(t)| < S_{\text{lim}}, \quad (6)$$

where G_{lim} and S_{lim} is the maximum gradient and slew rate amplitude constrained by the hardware, respectively.

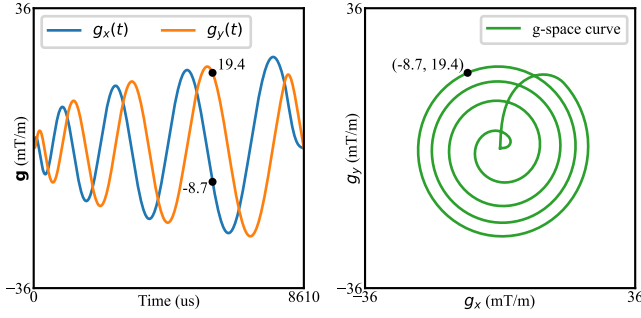


Fig. 1. Illustration of projecting example gradient waveforms to g -space where the coordinates are the gradients along the x - and y -directions.

B. Trajectory Definition

Any k -space trajectory in MRI can be parameterized as

$$\mathbf{k}(p) = (f(p), g(p), h(p)), \quad (7)$$

where p is a trajectory parameter, f, g, h are arbitrary scalar functions. For example, for a 2D spiral trajectory, p denotes the azimuthal angle θ , $f(p)$ and $g(p)$ denote the coordinates of the spiral trajectory, $h(p)$ is always zero, yielding

$$\mathbf{k}(p) = (Ap \cos p, Ap \sin p, 0). \quad (8)$$

Our goal is to find a gradient waveform $\mathbf{g}(t)$ such that its integral traces the curve defined by Eq. 7, while satisfying the constraints in Eq. 6.

C. Introduction to g -Space

G -space is defined as the space of gradient vectors \mathbf{g} with the coordinates being the gradients along the three spatial directions. The projection of an example gradient waveform into the corresponding g -space is illustrated in Fig. 1.

Given the gradient vector $\mathbf{g}(t_{\text{this}})$ at certain time point t_{this} , the gradient vector $\mathbf{g}(t_{\text{next}})$ at the next time point t_{next} , and time step $\Delta t = t_{\text{next}} - t_{\text{this}}$, if Δt is small enough, the slew rate amplitude within $(t_{\text{this}}, t_{\text{next}}]$ can be approximated as $|\mathbf{g}(t_{\text{next}}) - \mathbf{g}(t_{\text{this}})|/\Delta t$. The slew rate amplitude and the gradient amplitude at t_{next} ($|\mathbf{g}(t_{\text{next}})|$) should satisfy the hardware constraints in Eq. 6:

$$\forall t_{\text{next}} : |\mathbf{g}(t_{\text{next}})| < G_{\text{lim}}, \quad |\mathbf{g}(t_{\text{next}}) - \mathbf{g}(t_{\text{this}})| < S_{\text{lim}}\Delta t. \quad (9)$$

The two constraints for $\mathbf{g}(t_{\text{next}})$ can be considered as two circles in g -space (the blue and red circles in Fig. 2), with the radius being G_{lim} and $S_{\text{lim}}\Delta t$, respectively. Thus, the intersection region of the two circles defines the permissible region for the next gradient vector $\mathbf{g}(t_{\text{next}})$.

In addition to the hardware constraints, another constraint is that the next gradient $\mathbf{g}(t_{\text{next}})$ should be parallel to the tangent of the next trajectory sample (hereafter referred as the $d\mathbf{k}$ constraint):

$$\mathbf{g}(t_{\text{next}}) \parallel \left. \frac{d\mathbf{k}}{dp} \right|_{t_{\text{next}}}. \quad (10)$$

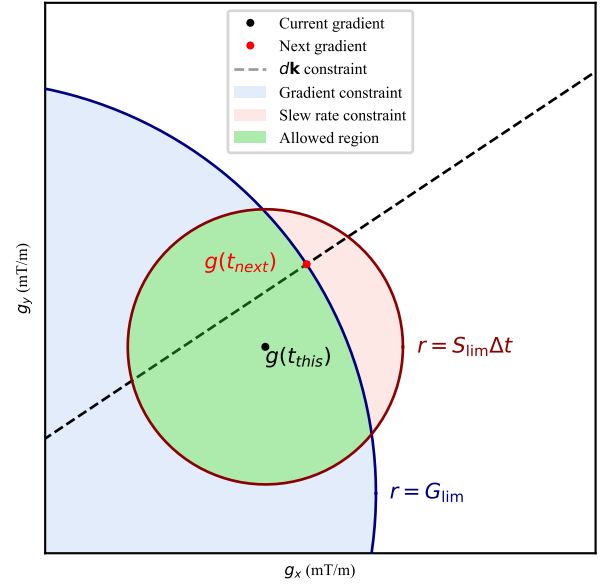


Fig. 2. The permissible region (in green) for the next gradient vector is the intersection of the gradient constraint region $|\mathbf{g}| < G_{\text{lim}}$ (in blue) and the slew rate constraint region $|\mathbf{g} - \mathbf{g}(t_{\text{this}})| < S_{\text{lim}}\Delta t$ (in red). The dashed line denotes all possible gradient vectors parallel to $d\mathbf{k}(t_{\text{this}})$.

Assuming Δt is sufficiently small, the tangent at the current trajectory sample is close to that at the next sample:

$$\frac{d\mathbf{k}(p_{\text{next}})}{dp} \approx \frac{d\mathbf{k}(p_{\text{this}})}{dp}, \quad (11)$$

where $p_{\text{this}} = p(t_{\text{this}})$ and $p_{\text{next}} = p(t_{\text{next}})$, which yields:

$$\mathbf{g}(t_{\text{next}}) \parallel \frac{d\mathbf{k}(p_{\text{this}})}{dp}. \quad (12)$$

The $d\mathbf{k}$ constraint is depicted as the dashed line in Fig. 2.

D. Recursive g -Space Solution

As introduced in the previous subsection, the direction of the next gradient vector is parallel to $d\mathbf{k}(t_{\text{this}})/dp$, thus

$$\hat{\mathbf{g}}(t_{\text{next}}) = \frac{d\mathbf{k}(p_{\text{this}})/dp}{|d\mathbf{k}(p_{\text{this}})/dp|} \text{sgn} \left(\frac{dp(t_{\text{this}})}{dt} \right), \quad (13)$$

where $\hat{\mathbf{g}}(t_{\text{next}})$ denotes the unit vector of $\mathbf{g}(t_{\text{next}})$.

Since a time-optimal gradient waveform must maximize either the gradient amplitude or the slew rate amplitude [12], the norm of the next gradient vector can be determined by solving for the farthest intersection between the slew rate constraint $|\mathbf{g} - \mathbf{g}(t_{\text{this}})| < S_{\text{lim}}\Delta t$ and the $d\mathbf{k}$ constraint $\mathbf{g}(t_{\text{next}}) \parallel d\mathbf{k}(t_{\text{this}})/dp$, subject to the maximum gradient amplitude G_{lim} , which is a simple graphical problem: finding the intersection of the line defined by $\mathbf{g}(t_{\text{next}}) \parallel d\mathbf{k}(t_{\text{this}})/dp$ and the circle defined by $|\mathbf{g} - \mathbf{g}(t_{\text{this}})| < S_{\text{lim}}\Delta t$. The solution is given by:

$$|\mathbf{g}(t_{\text{next}})| = \min \left\{ \frac{-b + \sqrt{b^2 - 4ac}}{2a}, G_{\text{lim}} \right\}, \quad (14)$$

where

$$\begin{aligned} a &= 1, \\ b &= -2\langle \mathbf{g}(t_{\text{this}}), \hat{\mathbf{g}}(t_{\text{next}}) \rangle, \\ c &= |\mathbf{g}(t_{\text{this}})|^2 - S_{\text{lim}}^2 \Delta t^2. \end{aligned}$$

Note that $\langle \cdot, \cdot \rangle$ denotes the inner product of two vectors.

The final solution for $\mathbf{g}(t_{\text{next}})$ is:

$$\mathbf{g}(t_{\text{next}}) = \hat{\mathbf{g}}(t_{\text{next}}) |\mathbf{g}(t_{\text{next}})|. \quad (15)$$

The second-order Runge–Kutta (RK2) approximation for $p(t_{\text{next}})$ is

$$p(t_{\text{next}}) = p(t_{\text{this}}) + \frac{(k_1 + k_2)dl}{2}, \quad (16)$$

where

$$\begin{aligned} dl &= |\mathbf{g}(t_{\text{next}})| \Delta t, \\ k_1 &= \left| \frac{dp}{d\mathbf{k}(p_{\text{this}})} \right| \text{sgn} \left(\frac{dp}{dt} \right), \\ k_2 &= \left| \frac{dp}{d\mathbf{k}(p_{\text{this}} + k_1 dl)} \right| \text{sgn} \left(\frac{dp}{dt} \right). \end{aligned}$$

By running the above steps recursively, a gradient sequence $\{\mathbf{g}(t_i) \mid i = 0, 1, \dots, N\}$ and a parameter sequence $\{p(t_i) \mid i = 0, 1, \dots, N\}$ can be obtained simultaneously. In Meyer's method [11], the gradient sequence is used as the final gradient waveform.

E. Limitations of the Existing Graphical Method

Since the mathematical relationships between trajectory, gradient, and slew rate are analogous to displacement, velocity, and acceleration in kinematic control, from this point onward we integrate these concepts into explaining the graphical solution.

The solution derived in the preceding sections is a generalization of the Meyer's graphical method [11], which is suitable for trajectories with monotonically decreasing curvature such as the spiral-out trajectory. However, this method cannot handle trajectories with increasing curvature as according to the gradient solution in Eq. 14, the gradient amplitude can only increase until the maximum value which may eventually exceed the escape velocity at certain point of the trajectory, resulting in an unsolvable problem for the graphical method. Moreover, constraining the next gradient to be parallel to the current k -space trajectory tangent does not strictly guarantee trajectory accuracy, which means the k -space sampling points defined by the designed gradients may deviate from the provided trajectory function.

To address these limitations, we first clarify the interpretation of the intersections between the slew rate constraint circle and the $d\mathbf{k}$ constraint line in Fig. 2:

- 1) *Two intersections*: The farther intersection corresponds to the velocity (gradient) of the k -space trajectory, where part of the slew rate is used for centripetal acceleration and the remainder for tangential acceleration. In contrast, at the nearer intersection, part of the slew rate is used for centripetal acceleration and the remainder for tangential deceleration.

- 2) *Single intersection*: Indicates that the maximum permitted slew rate is just sufficient to provide the required centripetal acceleration.
- 3) *No intersection*: Indicates that the available slew rate is insufficient to provide the required centripetal acceleration at the current curvature and speed (gradient).

If Meyer's method is applied to trajectories where curvature may increase, there will be no intersection near the curvature maxima. Although one can take the real part of the solution in Eq. 14, slew rate errors will be introduced.

F. Forward and Backward Sweep Strategy

The first problem we need to address is how to make the gradient amplitude decrease at an appropriate position before reaching the maximum curvature, so that solution to Eq. 14 always exists.

FBS strategy takes the minimum of the forward solution and the backward solution, denoted as:

$$\forall p: |\mathbf{g}(p)| = \min\{|\mathbf{g}_{\text{forw}}(p)|, |\mathbf{g}_{\text{back}}(p)|\}, \quad (17)$$

To integrate FBS into our method, gradients are first solved in backwards, where the gradient amplitude is constrained by both hardware limits and the escape velocity, as shown below:

$$|\mathbf{g}_{\text{back}}(p)| = \min \left\{ \frac{-b + \sqrt{b^2 - 4ac}}{2a}, G_{\text{lim}}, G_{\text{esc}} \right\}. \quad (18)$$

where G_{esc} is the escape velocity of the current trajectory sample, defined by:

$$G_{\text{esc}} = \sqrt{S_{\text{lim}} \left(\frac{d\mathbf{k}}{dp} \right)^3 / \left(\frac{d\mathbf{k}}{dp} \times \frac{d^2\mathbf{k}}{dp^2} \right)} \quad (19)$$

In the subsequent forward sweep, the gradient will be limited by the backward solution, allowing the k -space sample to decelerate appropriately near the curvature maxima, as shown below:

$$|\mathbf{g}_{\text{forw}}(p)| = \min \left\{ \frac{-b + \sqrt{b^2 - 4ac}}{2a}, |\mathbf{g}_{\text{back}}(p)| \right\}. \quad (20)$$

This approach ensures that, near regions of high curvature, the gradient amplitude in the forward sweep will decrease at the same slew rate as in the backward sweep, i.e., the maximum available slew rate. Therefore, the FBS strategy guarantees that the gradient waveform not only operates at the maximum slew rate for time-optimality, but also remains below the escape velocity – even at curvature maxima – ensuring that Eq. 14 always has a solution.

G. Reparameterization

Another problem is how to ensure that the k -space sampling pattern derived from the designed gradient waveforms exactly follows the desired trajectory. Based on the recursive algorithm introduced in Sec. II-D, we obtain two sequences after the

TABLE I
OUTLINE OF THE PROPOSED ALGORITHM

OUTLINE OF THE PROPOSED ALGORITHM	
INPUTS: $\mathbf{k}(p)$, $p \in [P_0, P_1]$ – Parameter function defining the desired trajectory. G_{\lim}, S_{\lim} – Gradient amplitude and slew rate amplitude limit. G_0, G_1 – Initial and final gradient amplitude. Δt – Time step size.	
OUTPUTS: $\mathbf{g}[i], p[i]$ – Gradient sequence and corresponding trajectory parameter sequence.	
ALGORITHM: <ol style="list-style-type: none"> 1) Backward sweep <ol style="list-style-type: none"> a) Initialize: $\text{Define: } i = 0, s_{pt} = \text{sgn}\left(-\frac{dp}{dt}\right), p[i] = P_1, \mathbf{g}[i] = s_{pt}G_1 \frac{d\mathbf{k}(p[i])/dp}{ d\mathbf{k}(p[i])/dp }$ b) Compute the direction of next gradient vector: $\hat{\mathbf{g}}[i+1] \leftarrow \frac{d\mathbf{k}(p[i])/dp}{ d\mathbf{k}(p[i])/dp } s_{pt}$ c) Compute the norm of next gradient vector by solving the line-circle intersection: $a \leftarrow 1, b \leftarrow -2\langle \mathbf{g}[i], \hat{\mathbf{g}}[i+1] \rangle, c \leftarrow \mathbf{g}[i] ^2 - S_{\lim}^2 \Delta t^2$ $\mathbf{g}[i+1] \leftarrow \frac{-b + \sqrt{b^2 - 4ac}}{2a}$ d) Limit the norm of next gradient vector under hardware constraint and escape velocity: $G_{\text{esc}} \leftarrow \sqrt{S_{\lim} \left(\frac{d\mathbf{k}}{dp}\right)^3 / \left(\frac{d\mathbf{k}}{dp} \times \frac{d^2\mathbf{k}}{dp^2}\right)}$ $\mathbf{g}[i+1] \leftarrow \min\{ \mathbf{g}[i+1] , G_{\lim}, G_{\text{esc}}\}$ e) Update next gradient vector: $\mathbf{g}[i+1] \leftarrow \hat{\mathbf{g}}[i+1] \mathbf{g}[i+1]$ f) Update for p using RK2: $p[i+1] \leftarrow p[i] + \mathbf{g}[i+1] \Delta t \cdot s_{pt} \left(\left \frac{dp}{d\mathbf{k}(p[i])} \right + \left \frac{dp}{d\mathbf{k}(p[i] + k_1 dl)} \right \right) / 2$ g) Update index: $i \leftarrow i + 1$ h) Repeat steps b–g until $p[i+1] < \min\{P_0, P_1\}$ or $p[i+1] > \max\{P_0, P_1\}$. i) Interpolate the gradient amplitude sequence: $\mathbf{g}_{\text{back}} (p) \leftarrow \text{intp}(p, \mathbf{g})$ 2) Forward sweep <ol style="list-style-type: none"> a) Initialize: $\text{Define: } i = 0, s_{pt} = \text{sgn}\left(\frac{dp}{dt}\right), p[i] = P_0, \mathbf{g}[i] = s_{pt}G_0 \frac{d\mathbf{k}(p[i])/dp}{ d\mathbf{k}(p[i])/dp }$ b) Compute the direction of next gradient vector with the formula provided in the backward step. c) Compute the norm of next gradient vector by solving the line-circle intersection. d) Limit the norm of next gradient vector under the backward solution: $\mathbf{g}[i+1] \leftarrow \min\{ \mathbf{g}[i+1] , \mathbf{g}_{\text{back}} (p[i])\}$ e) Update the next gradient vector. f) Update for p using RK2. g) Update index. h) Repeat steps b–g until $p[i+1] < \min\{P_0, P_1\}$ or $p[i+1] > \max\{P_0, P_1\}$. 3) Reparameterization <ol style="list-style-type: none"> a) Derive trajectory by evaluating function $\mathbf{k}(p)$ at $p[i]$ $\mathbf{k}[i] \leftarrow \mathbf{k}(p[i])$ b) Derive gradient waveform by differentiating the trajectory $\mathbf{g}[i] \leftarrow (\mathbf{k}[i+1] - \mathbf{k}[i]) / \Delta t$ 	

TABLE II
SUMMARY OF THE IMAGING PARAMETERS FOR PHANTOM AND IN-VIVO EXPERIMENTS.

Trajectory	Res (mm)	FOV (mm)	FA (deg)	BW (Hz)	Grad (mT/m)	Slew (T/m/s)	TE (ms)	TR (ms)	Scan Time (s)
Spiral	0.5	256	10	–	50	50	1.25	14.01	2.86
Variable Density Spiral	0.5	256	10	–	50	50	1.25	12.73	5.19
Rosette	0.5	256	10	–	50	50	(Mixed)	20.35	6.53
Cartesian (2D)	0.5	256	10	500	–	–	4.21	9.00	4.61
Yarnball	1.0	256	10	–	50	50	1.10	16.19	265.26
Cones	1.0	256	10	–	50	50	1.10	12.10	297.44
Seiffert Spiral	1.0	256	10	–	50	50	1.10	14.65	317.64
Stack-of-Spiral	1.0	256	10	–	50	50	1.10	12.10	198.25
Cartesian (3D)	1.0	256	10	500	–	–	2.88	6.90	452.20

Res: resolution; FOV: field of view; FA: flip angle; BW: bandwidth; Grad: gradient amplitude limit; Slew: slew rate amplitude limit; TE: echo time; TR: repetition time. "–" indicates not applicable.

solving process: $\mathbf{g}(t_i)$ and $p(t_i)$. Therefore, there are two approaches to derive the final gradient waveform:

- 1) Use $\mathbf{g}(t_i)$ directly as described in Meyer's method [11].
- 2) Evaluate the trajectory function at $p(t_i)$ to obtain $\mathbf{k}(t_i)$, and then reparameterize $\mathbf{g}(t_i)$ by taking the derivative of $\mathbf{k}(t_i)$, which is referred to as reparameterization.

The first approach ensures exact hardware constraints based on the properties of g -space, while the second approach ensures exact sampling accuracy which is preferred over the first approach for trajectory fidelity. The reparameterization approach may lead to a trade-off in slew rate accuracy, which can be compensated for by employing temporal oversampling by using a smaller time step than the actual trajectory time step during the recursive g -space solving process. The outputted gradient waveform is then downsampled before being passed to the gradient hardware. The proposed method is summarized in Table. I.

H. Code Availability

The implementation of the proposed method, as well as example scripts and data for reproducing the main results will be publicly available at <https://github.com/RyanShanghaitech/MrAutoGrad> upon publication of this study.

III. EXPERIMENTS

To evaluate the computation speed and slew rate control accuracy, simulation experiments were performed using both the proposed g -space solver and the previous optimal-control solver [12] for designing the commonly adopted 2D and 3D non-Cartesian trajectories [7], [10], [20], [21]. To assess the feasibility and imaging quality of the proposed method in a practical setting, the proposed method was implemented in a 3.0-T United Imaging MR scanner for phantom and in-vivo non-Cartesian imaging.

A. Simulations

The reparameterization strategy adopted to ensure trajectory accuracy introduces a tunable parameter, the temporal oversampling factor, which controls the trade-off between slew rate control accuracy and computational speed. Simulations were performed to optimize this parameter for a representative

2D non-Cartesian trajectory, Rosette, and a 3D non-Cartesian trajectory, Yarnball.

The proposed method was compared with the widely adopted optimal-control method for designing time-optimal gradient waveforms for a range of non-Cartesian trajectories including Archimedean Spiral, Variable Density Spiral, Rosette [10], Yarnball [20], Cones [21], Seiffert Spiral [7], and Stack-of-Spiral. Both the proposed method and the previous optimal-control method were implemented in C++. The code for the optimal-control method was adapted from the official implementation¹ with minimal trivial modifications for compatibility. Hereafter, we refer to the proposed method as **MRAutoGrad (MAG)**, reflecting our library name, and to the previous optimal-control method as **MinTimeGrad (MTG)**, following the name of its original software implementation.

During the simulation, the slew rate amplitude was limited to 50 T/m/s for the balance between imaging speed and quality, and the gradient amplitude was limited to 20 mT/m. Each trajectory was simulated ten times to calculate the mean computation time. For evaluating the slew rate control accuracy, the slew rate overshoot was calculated as follows:

$$\text{Overshoot} = \frac{\max_i \{s[i]\} - S_{\text{lim}}}{S_{\text{lim}}} \times 100\% \quad (21)$$

B. Imaging Experiments

To evaluate the non-Cartesian imaging performance with the gradient waveforms generated by the proposed MAG solver, phantom and in-vivo imaging experiments were conducted by imaging the NIST/ISMRM phantom (System Phantom, Model 130 from CaliberMRI®) and the knee of a healthy subject after IRB approval and informed consent. The slew rate amplitude limit was consistent with that used in the simulation, while the gradient amplitude limit was relaxed to 50 mT/m to increase the imaging speed. The non-Cartesian MR reconstruction was performed using non-uniform fast Fourier transform (NUFFT) [22], [23], where the sampling density compensation function was calculated using a numerical iterative method [24]. Imaging parameters are summarized in Table II. It is noted that a 1-3-3-1 water-excitation pulse was adopted to suppress the fat

¹Refer to the "Time Optimal Gradient Design" section at <https://people.eecs.berkeley.edu/~mlustig/Software.html>

TABLE III

COMPARISON OF COMPUTATION TIME AND SLEW RATE OVERSHOOT FOR THE MTG AND PROPOSED MAG METHODS.

Trajectory	MTG Exe. Time [ms] (mean \pm std)	MAG Exe. Time [ms] (mean \pm std)	Time Reduction	MTG Slew Overshoot [%]	MAG Slew Overshoot [%]	Overshoot Reduction
Spiral	88.149 \pm 6.848	20.593 \pm 0.555	76.639%	4.128	0.034	99.176%
Variable Density Spiral	64.262 \pm 3.391	18.701 \pm 0.356	70.899%	4.065	0.038	99.065%
Rosette	184.782 \pm 9.494	48.327 \pm 3.776	73.847%	4.152	0.050	98.796%
Yarnball	23144.284 \pm 79.914	6662.080 \pm 20.862	71.215%	4.152	0.035	99.157%
Cones	24387.079 \pm 98.139	7731.312 \pm 56.214	68.298%	4.151	0.037	99.109%
Seiffert Spiral	144.468 \pm 6.711	193.602 \pm 5.132	-34.010%	4.084	0.038	99.070%
Stack-of-Spiral	106.788 \pm 11.042	24.486 \pm 5.604	77.070%	4.128	0.034	99.176%

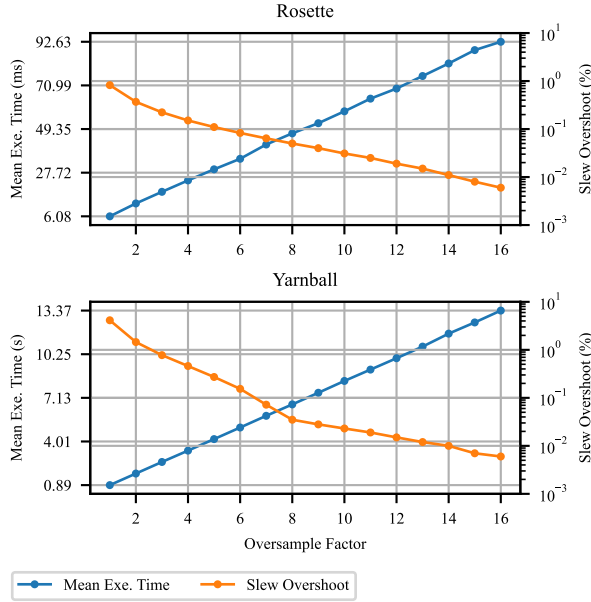


Fig. 3. Mean execution time and slew rate overshoot versus oversampling factor in Rosette and Yarnball trajectory.

signal for all the non-Cartesian imaging sequences. However, for the Cartesian imaging, the number of repetitions can be significantly larger than the non-Cartesian imaging, which may lead to prohibitively long scan duration if adopting the water excitation pulse, that extends the repetition time significantly, so the water excitation was not adopted for the Cartesian imaging sequences.

IV. RESULTS

A. Simulations

The influence of the temporal oversampling factor on the computation time and slew rate control accuracy for the proposed method is demonstrated in Fig. 3. It can be seen that too small a value results in obvious slew rate overshoot, while too large a value leads to overlong computation time. A temporal oversampling factor of 8 achieves a good trade-off between slew rate control accuracy and computation speed, which was adopted in the following experiments with the proposed method.

Fig. 6 compares the designed gradient waveforms, gradient and slew rate amplitudes, and slew rate overshoot percentages for the proposed MAG solver and the previous MTG solver

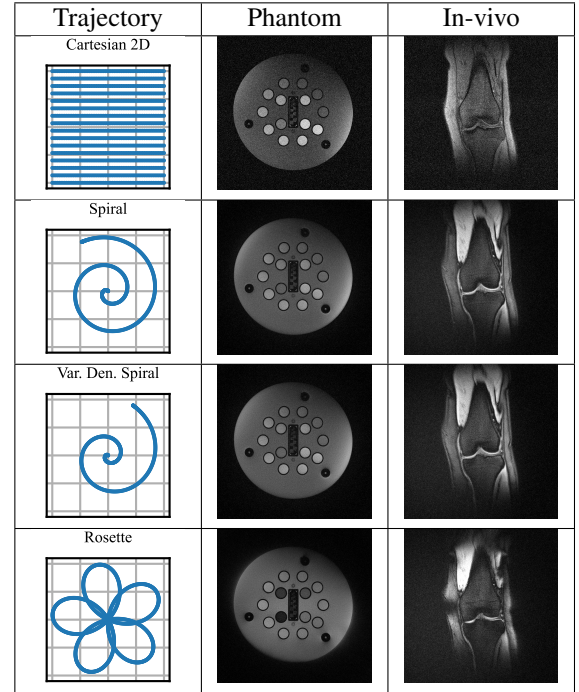


Fig. 4. The phantom and in-vivo images acquired with three 2D non-Cartesian trajectories implemented using MAG in comparison with the images acquired with Cartesian sampling.

across different 2D and 3D non-Cartesian trajectories. Both methods are able to generate time-optimal gradient waveforms under the gradient amplitude constraint of 20 mT/m and slew rate amplitude constraint of 50 T/m/s. However, the MTG solver tends to have slew rate overshoot at the beginning of the trajectory, where the proposed method has better control of the slew rate, achieving close-to-zero slew rate overshoot for all simulated trajectories.

Furthermore, the MAG solver is more efficient than the MTG solver which involves additional computation to convert other trajectory parameterization to arc-length parameterization, and achieved a substantial reduction in computation time for almost all trajectories as summarized in Table III. With the current implementation, the proposed method requires frequent evaluation of the trajectory function for calculating trajectory derivatives. The Seiffert Spiral trajectory is defined based on Jacobi elliptic functions, the evaluation of which is more time-consuming than other trajectories defined with elementary functions, leading to slightly longer computation time of the proposed method than MTG for this trajectory. It

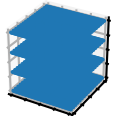

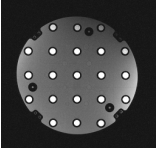
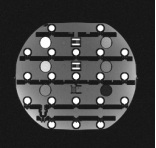

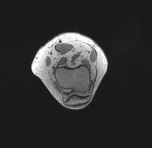
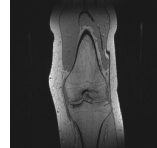


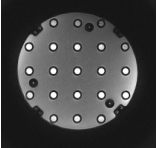
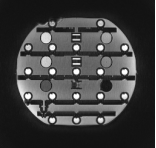
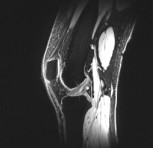
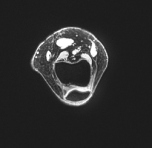
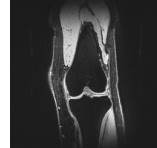
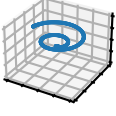

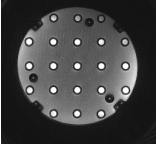
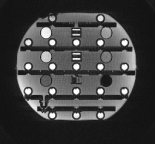
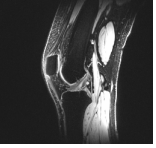
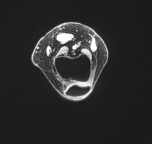
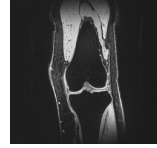
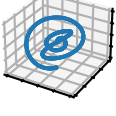
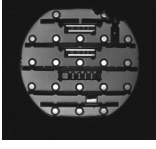
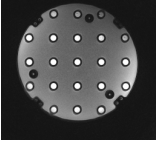
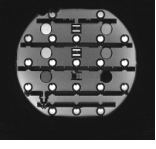
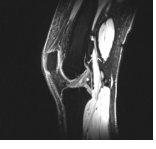
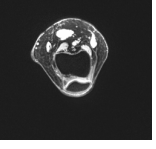
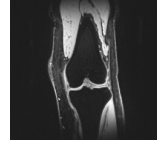
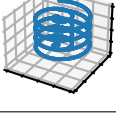
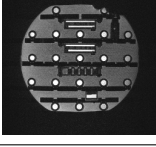
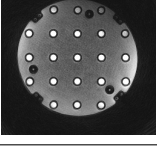
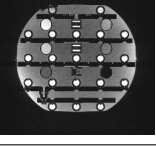

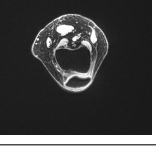
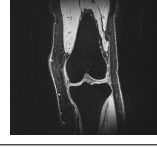
Trajectory	SAG	TRA	COR	SAG	TRA	COR
Cartesian 3D 						
Yarnball 						
Cones 						
Seiffert Spiral 						
Stack-of-Spiral 						

Fig. 5. The phantom and in-vivo images acquired with four 3D non-Cartesian trajectories implemented using MAG in comparison with the images acquired with Cartesian sampling. SAG: sagittal; TRA: transverse; COR: coronal; Column 2~4 are the phantom images, column 5~7 are the in-vivo images.

is also noted that it took much longer for designing the time-optimal gradient waveforms for Yarnball and Cones than other trajectories. This is because Yarnball and Cones have unique sampling for each interleaf and the gradients need to be solved for all interleaves, while others have only one unique interleaf shape, requiring running the gradient solver only once.

B. Phantom and In vivo Experiments

The 2D and 3D imaging results of the phantom and human knee are respectively presented in Fig. 4 and Fig. 5. All the non-Cartesian acquisitions with the readout gradients designed by the proposed MAG solver were successfully performed, generating images depicting clear anatomical structures and free of distortions using the Cartesian acquisitions as reference. Note that the data acquired with the Rosette trajectory has multiple echoes, and averaging the multi-echo data may cause signal cancellation for certain tissues, leading to dark regions in the Rosette image.

V. DISCUSSION & CONCLUSION

The proposed method achieves substantial reductions in both execution time and slew rate overshoot compared to the currently mainstream method based on optimal-control theory. Reducing execution time is especially important for trajectories with unique interleaf per TR, such as Yarnball

and Cones. In these cases, the gradient waveforms need to be designed for each interleaf separately, which may take prohibitively long computation time for the previous optimal-control method (MTG), particularly on MR system with a low-performance computer. Furthermore, for real-time imaging with highly randomized trajectories such as the randomly undersampled Yarnball, where each interleaf has a unique shape parameter, it is impossible to generate any interleaf by simply translating or rotating previous ones. In such scenario, real-time gradient computation is required. Our proposed method meets the challenging requirement by achieving the computation time for a single Yarnball interleaf of 6.55 ms on a 4 GHz computer, which is well under the corresponding TR of 11.12 ms. Additionally, precise slew rate control is crucial for maintaining pulse sequences within hardware constraints while facilitating the reliable clinical implementation of non-Cartesian imaging protocols. Although a $\sim 4\%$ slew rate overshoot of the previous MTG may not necessarily cause noticeable image quality degradation, it can lead to scan failure when the slew rate limit is set close to the hardware limit for fast imaging.

Another advantage of our method is that the final gradient is derived by differentiating the trajectory derived from the parameter sequence, so that each gradient vector has a corresponding trajectory parameter. This is particularly useful when

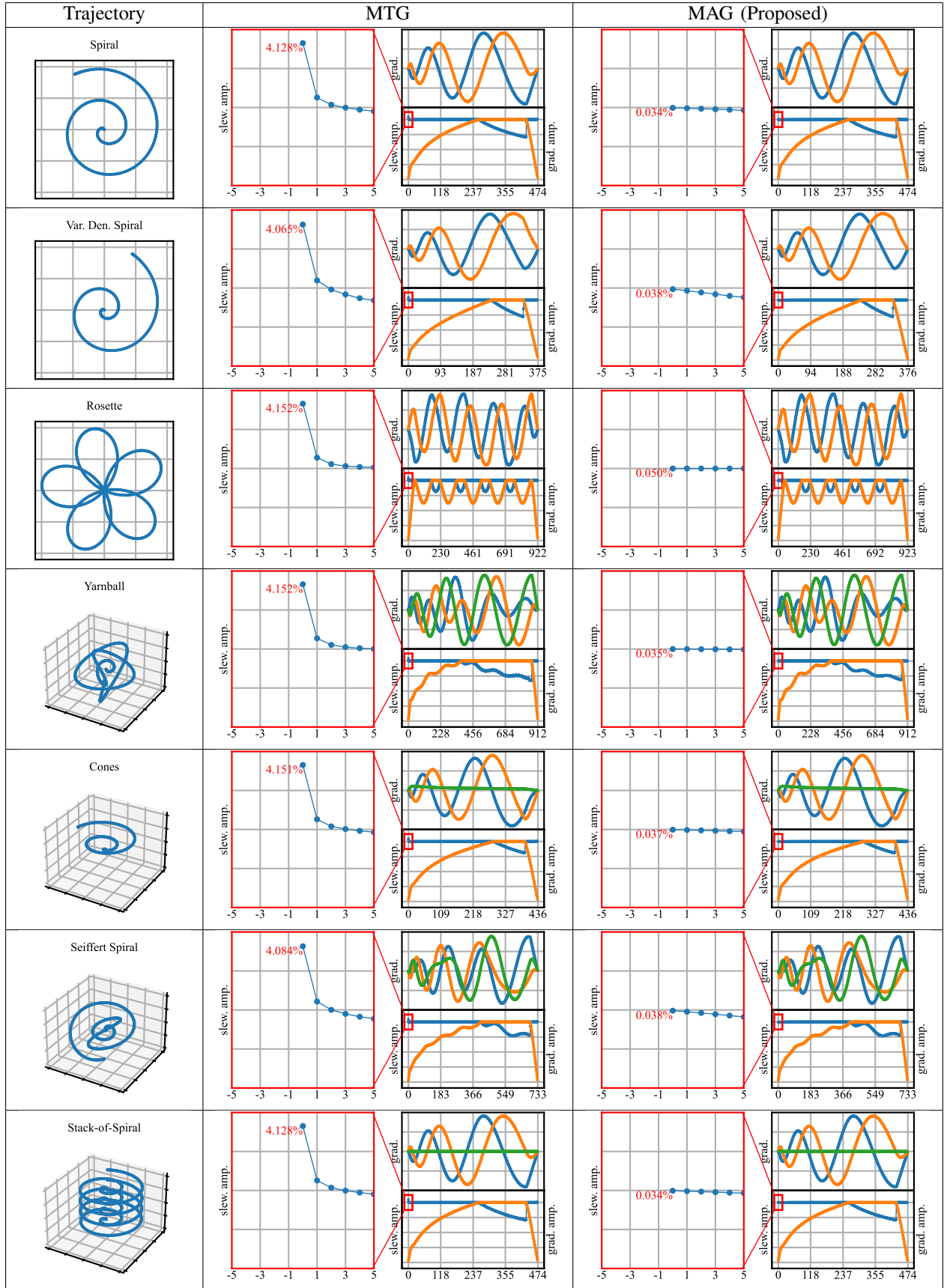


Fig. 6. Visualization of the gradient waveforms and the corresponding gradient amplitude, slew rate generated by MTG and MAG for various 2D and 3D non-Cartesian trajectories. The initial part of the slew rate curve is zoomed in for comparing the slew rate overshoot percentages between MTG and MAG. In the right-top subfigure, the blue, orange and green curve represents the x-, y-, and z-channel gradient, respectively. In the right-bottom subfigure, the blue and orange curve represents the corresponding slew rate and gradient amplitude, respectively.

readout segmentation is needed, such as in the Rosette acquisition, where multi-echo data can be separated to construct images with different TEs.

Although the graphical representation of gradient waveforms was previously explored in Meyer's method [11], that approach is specifically designed for spiral trajectory and cannot be generalized to arbitrary non-Cartesian trajectories. We introduce the Forward and Backward Sweep strategy to make the graphical method applicable to designing time-optimal gradient waveforms for all kinds of imaging trajectories. Furthermore, the previous method does not guarantee the accuracy of generated trajectories, and a reparameterization strategy is designed to ensure k-space trajectory fidelity.

The advantages of our approach over the previous Lustig's method (MTG) are faster computation speed and better slew rate control as have been validated in simulations. The subsequent imaging experiments were aimed to demonstrate the feasibility of the time-optimal gradient waveforms designed by the proposed method (MAG) for 2D and 3D phantom and in-vivo non-Cartesian imaging. Since similar imaging quality can be expected for the two gradient design methods, efforts were not made to implement the previous MTG method in the scanner for actual MR scan. However, the conventional Cartesian imaging was performed as the reference for image quality.

In summary, a fast general graphical method has been proposed for designing time-optimal gradient waveforms for arbitrary k-space trajectories. Compared with the state-of-the-art optimal-control method, the proposed method achieves a significant reduction of computation time and better slew rate control for a wide range of non-Cartesian trajectories, facilitating rapid gradient calculation for real-time MRI applications. We have demonstrated the feasibility of the proposed gradient design method for 2D and 3D non-Cartesian imaging of phantom and human knee.

REFERENCES

- [1] D. Ma *et al.*, "Magnetic resonance fingerprinting," *Nature*, vol. 495, no. 7440, pp. 187–192, Mar. 2013.
- [2] J. I. Hamilton, W. Truesdell, M. Galizia, N. Burris, P. Agarwal, and N. Seiberlich, "A low-rank deep image prior reconstruction for free-breathing ungated spiral functional CMR at 0.55 T and 1.5 T," *Magn Reson Mater Phy*, vol. 36, no. 3, pp. 451–464, Apr. 2023.
- [3] C. Lazarus *et al.*, "SPARKLING: Variable-density k-space filling curves for accelerated T2*-weighted MRI," *Magn. Reson. Med.*, vol. 81, no. 6, pp. 3643–3661, 2019.
- [4] Z. Zhou, A. Alfayad, T. C. Chao, and J. G. Pipe, "Acoustic noise reduction for spiral MRI by gradient derating," *Magn. Reson. Med.*, vol. 90, no. 4, pp. 1547–1554, 2023.
- [5] S. Blömer *et al.*, "Proton-free induction decay MRSI at 7T in the human brain using an egg-shaped modified rosette K-space trajectory," *Magn Reson Med*, vol. 93, no. 4, pp. 1443–1457, Apr. 2025.
- [6] P. F. Ferreira, P. D. Gatehouse, R. H. Mohiaddin, and D. N. Firmin, "Cardiovascular magnetic resonance artefacts," *Journal of Cardiovascular Magnetic Resonance*, vol. 15, no. 1, p. 41, Jan. 2013.
- [7] T. Speidel, P. Metzke, and V. Rasche, "Efficient 3D Low-Discrepancy k-Space Sampling Using Highly Adaptable Seifert Spirals," *IEEE Trans. Med. Imag.*, vol. 38, no. 8, pp. 1833–1840, Aug. 2019.
- [8] D.-h. Kim, E. Adalsteinsson, and D. M. Spielman, "Simple analytic variable density spiral design," *Magn. Reson. Med.*, vol. 50, no. 1, pp. 214–219, 2003.
- [9] C. Salustri, Y. Yang, and G. Glover, "Simple but Reliable Solutions for Spiral MRI Gradient Design," *Journal of Magnetic Resonance*, vol. 140, no. 2, pp. 347–350, Oct. 1999.
- [10] D. Noll, "Multishot rosette trajectories for spectrally selective MR imaging," *IEEE Trans. Med. Imag.*, vol. 16, no. 4, pp. 372–377, Aug. 1997.
- [11] C. H. Meyer and J. M. Pauly, "Rapid method of optimal gradient waveform design for MRI," US Patent US6 020 739A, Feb., 2000.
- [12] M. Lustig, S.-J. Kim, and J. M. Pauly, "A fast method for designing time-optimal gradient waveforms for arbitrary k-space trajectories," *IEEE Trans. Med. Imag.*, vol. 27, no. 6, pp. 866–873, Jun. 2008.
- [13] L. Kasper *et al.*, "Matched-filter acquisition for BOLD fMRI," *NeuroImage*, vol. 100, pp. 145–160, Oct. 2014.
- [14] S. J. Malik and J. V. Hajnal, "Phase relaxed localized excitation pulses for inner volume fast spin echo imaging," *Magn. Reson. Med.*, vol. 76, no. 3, pp. 848–861, 2016.
- [15] S. J. Vannesjo *et al.*, "Image reconstruction using a gradient impulse response model for trajectory prediction," *Magn. Reson. Med.*, vol. 76, no. 1, pp. 45–58, 2016.
- [16] N. Chauffert, P. Weiss, J. Kahn, and P. Ciuciu, "A Projection Algorithm for Gradient Waveforms Design in Magnetic Resonance Imaging," *IEEE Trans. Med. Imag.*, vol. 35, no. 9, pp. 2026–2039, Sep. 2016.
- [17] M. Davids, M. Ruttorf, F. G. Zöllner, and L. R. Schad, "Fast and Robust Design of Time-Optimal k-Space Trajectories in MRI," *IEEE Trans. Med. Imag.*, vol. 34, no. 2, pp. 564–577, Feb. 2015.
- [18] O. P. Simonetti, J. L. Duerk, and V. Chankong, "MRI gradient waveform design by numerical optimization," *Magn. Reson. Med.*, vol. 29, no. 4, pp. 498–504, Apr. 1993.
- [19] O. Simonetti, J. Duerk, and V. Chankong, "An optimal design method for magnetic resonance imaging gradient waveforms," *IEEE Trans. Med. Imag.*, vol. 12, no. 2, pp. 350–360, Jun. 1993.
- [20] R. W. Stobbe and C. Beaulieu, "Three-dimensional Yarnball k-space acquisition for accelerated MRI," *Magn. Reson. Med.*, vol. 85, no. 4, pp. 1840–1854, 2021.
- [21] P. T. Gurney, B. A. Hargreaves, and D. G. Nishimura, "Design and analysis of a practical 3D cones trajectory," *Magn. Reson. Med.*, vol. 55, no. 3, pp. 575–582, 2006.
- [22] A. H. Barnett, "Aliasing error of the $\exp(\beta\sqrt{1-z^2})$ kernel in the nonuniform fast Fourier transform," Oct. 2020, arXiv preprint arXiv:2001.09405.
- [23] A. H. Barnett, J. F. Magland, and L. af Klinteberg, "A parallel non-uniform fast Fourier transform library based on an "exponential of semicircle" kernel," Apr. 2019, arXiv preprint arXiv:1808.06736.
- [24] J. G. Pipe and P. Menon, "Sampling density compensation in MRI: Rationale and an iterative numerical solution," *Magn. Reson. Med.*, vol. 41, no. 1, pp. 179–186, 1999.